



A Polyoxoniobate/g-C₃N₄ Nanoporous Material with High Adsorption Capacity of Methylene Blue from Aqueous Solution

Qiuyun Gan¹, Weilong Shi², Yanjun Xing^{1*} and Yu Hou^{1*}

¹ College of Chemistry, Chemical Engineering and Biotechnology, Donghua University, Shanghai, China, ² Institute of Functional Nano and Soft Materials, Soochow University, Suzhou, China

OPEN ACCESS

Edited by:

Taohai Li,
Xiangtan University, China

Reviewed by:

Bahar Karadeniz,
Rudjer Boskovic Institute, Croatia
Shuiying Gao,
Institute of Chemistry (CAS), China

*Correspondence:

Yanjun Xing
yixing@dhu.edu.cn
Yu Hou
houyu@dhu.edu.cn

Specialty section:

This article was submitted to
Inorganic Chemistry,
a section of the journal
Frontiers in Chemistry

Received: 04 December 2017

Accepted: 10 January 2018

Published: 31 January 2018

Citation:

Gan Q, Shi W, Xing Y and Hou Y
(2018) A Polyoxoniobate/g-C₃N₄
Nanoporous Material with High
Adsorption Capacity of Methylene
Blue from Aqueous Solution.
Front. Chem. 6:7.
doi: 10.3389/fchem.2018.00007

A polyoxoniobate/g-C₃N₄ nanoporous material with functional groups has been synthesized by using carbon nitride (g-C₃N₄) and hexaniobate (K₈Nb₆O₁₉·10H₂O, abbreviated as NbO) as precursors. The structure and compositions of the as-prepared nanomaterials were characterized by XRD, FT-IR, FESEM, TEM, and XPS. These two kinds of materials interact with each other forming a hybrid composite, which can be used as an adsorbent for removing a cationic dye (methylene blue, MB) from wastewater with excellent adsorption capacity. Furthermore, parameters that can affect adsorption process including initial dye concentration, pH and temperature were investigated by batch adsorption experiments. The results indicated that the maximum adsorption capacity of NbO/g-C₃N₄ can reach up to 373.1 mg g⁻¹. Moreover, the equilibrium experiment data fitted Langmuir isotherm well and the adsorption kinetics showed that the pseudo second order model can satisfyingly described MB adsorption kinetics. The thermodynamic analysis indicated that the adsorption was endothermic and spontaneous.

Keywords: polyoxoniobate, carbon nitride, methylene blue, adsorption, nanoporous material

INTRODUCTION

Organic dyes has been a vital environmental pollution source since various industries use it in many fields, such as textile, leather, printing, dyestuff, and cosmetics (Liu X. X. et al., 2016; Cai et al., 2017). Among all dyes, methylene blue (MB), is one of the most common dyeing pollutants (Xu et al., 2017). The excessive emission of MB in the environment will induce eye burns, mental confusion, shock, and vomiting (Xu et al., 2017). Hence, it is exigent to develop effective materials to remove the MB from waste water.

In order to eliminate organic dyes from waste water, several methods including adsorption (Haque et al., 2011; Wang et al., 2016; Yan et al., 2016), photo-degradation (Kumar et al., 2014; He et al., 2015; Xin et al., 2017), chemical oxidation (Osugi et al., 2009), and biological treatment (Zhang et al., 2014) have been used. Compared to others, adsorption is considered as a most effective method due to its simple design and operation, high efficiency, and economy (Haque et al., 2011). To promote the removal efficiency, a variety of adsorbents have been synthesized for the removal of MB, such as activated carbon (Bestani et al., 2008), graphene (Liu et al., 2012), magnesium oxide (Moussavi and Mahmoudi, 2009; Hu et al., 2010), and polymer (Xiao et al., 2015). Recently, graphitic carbon nitride (g-C₃N₄), a structurally graphite-like material, has been widely studied in photocatalytic hydrogen production (Wang et al., 2012) and removing water pollutants (Wang et al., 2013) due to its low cost, outstanding physicochemical properties and excellent

chemical and thermal stability. However, reports on g-C₃N₄ as adsorbent to adsorb dyes was rare, mainly due to its low surface area, very limited functional groups and less binding sites. Peng and coworkers synthesized a series of mesoporous carbon nitride to adsorb MB and the adsorbents exhibited noteworthy effects (Peng et al., 2017). This study showed that g-C₃N₄ is able to remove organic dyes from the aqueous environment, and it is also a promising material for adsorption.

Polyoxometalates (POMs) has attracted extensive attention owing to their special structural properties and extensive applications in catalysis, medicine, and materials. They can also combine with other materials to modify the structure and properties of the materials (Troupis et al., 2002). Recently, a few studies on incorporating tungsten- and molybdenum- containing POMs into g-C₃N₄ have been reported (Li et al., 2014; Long et al., 2014; He et al., 2015; Liu J. H. et al., 2016; Zhao et al., 2017), such as PW₁₂O₄₀/g-C₃N₄, PMo₁₂O₄₀/g-C₃N₄, Co₄PW₉O₃₄/C₃N₄, g-C₃N₄/PW₁₁O₃₉, FePW₄O₂₄/g-C₃N₄, and PMo₁₀V₂O₄₀/C₃N₄. Results indicated that the polyanionic, highly redox-active and acidic properties of POMs significantly modified the properties of g-C₃N₄ and these hybrid materials showed great photocatalytic performances on degradation of dyes, water oxidation, and hydrocarbon oxidation. Polyoxoniobates (PONbs), a branch of POMs, were different from W-, Mo-, and V- containing POMs in both synthesis and aqueous solution behaviors. They have unique properties including high specific surface area, high charge, high alkalinity, and photocatalytic activity. These properties endow them with applications for photocatalysis of water splitting, based-catalyzed decomposition of contaminants, and biological activity (Wu et al., 2015). Thus, it would be very interesting to combine polyoxoniobate with g-C₃N₄ to see if PONb has different influence on the photocatalytic performance. Surprisingly, the prepared material shows great adsorption capacity for MB in aqueous solution when we attempt to use it as photocatalyst for degradation of dyes. To the best of our knowledge, no such material have been synthesized and tested for the adsorption of organic dyes.

In this study, we used a facile hydrothermal treatment method to synthesize NbO/g-C₃N₄ material with porous structure by using K₈Nb₆O₁₉·10H₂O (NbO) and g-C₃N₄ as precursors. And we choose MB as an adsorbate to explore the adsorption capacity of NbO/g-C₃N₄ material. The structural and chemical property of NbO/g-C₃N₄ was investigated, and the results showed that both of them have important influence on the performance of adsorption dyes. In addition, the effects of different parameters on MB adsorption by NbO/g-C₃N₄ were also investigated. We also studied the thermodynamics, adsorption isotherms, and kinetics of adsorption process. The results revealed that NbO/g-C₃N₄ is an efficient adsorbent for removing MB from waste water.

EXPERIMENTAL SECTION

Materials and Methods

Anhydrous niobium oxide (Nb₂O₅, ≥99.5%), potassium hydroxide (KOH, ≥85%), methylene blue (MB) were purchased from Sinopharm Chemical Reagent. Melamine (99%) was

obtained for Sigma-Aldrich. All the chemicals were used as received without further purification. The synthesis of NbO/g-C₃N₄ hybrid was completed by hydrothermal treatment method. Firstly, g-C₃N₄ was synthesized by direct heating melamine. Briefly, 5 g melamine powder was placed into an alumina crucible with a cover and heated to 550°C for 2 h at a rate of 10°C/min in a muffle furnace under air. After cooling to room temperature, the resulting yellow sample was obtained. NbO was prepared according to the previous literature and its identity was further confirmed by IR spectrum (Liu et al., 2015). Two hundred milligrams of NbO was dissolved in 15 mL distilled water, and then 184 mg of as-prepared g-C₃N₄ were added into the aqueous solution. The suspension was ultrasound continuously for 10 h. Finally, the resulting mixture transfer into a Teflon-lined stainless autoclave at 180°C for 24 h. The product was centrifuged, washed with distilled water, and dried at 60°C for 12 h.

Characterizations

The morphology of the samples was observed by using a field emission scanning electron microscope (FESEM, S-4800) and a transmission electron microscopy (TEM, JEM-2100) operating at 200 kV X-ray diffraction studies (XRD, D/max-2550VB+/PC) was carried out to determine the phase composition of the samples. The functional groups on the NbO/g-C₃N₄ surface were obtained on Fourier transform infrared spectroscopy (FTIR, Nicolet iS5). The FTIR spectra were recorded in the range 400–4000 cm⁻¹ using KBr pellets. The real chemical composition of the products was determined using X-ray photoelectron spectroscopy (XPS, ESCA Lab250). The concentration of the dye was determined on UV-Vis spectrophotometer (UV 210).

Adsorption Experiments

Adsorption experiments were carried out in Erlenmeyer flask (250 mL), where solution of MB (200 mL) with initial dye concentration of 10–40 mg L⁻¹ was placed. The flask with MB solution was sealed and placed in a constant temperature bath and agitated by magnetic stirrer. In order to investigate the effect of temperature, the experiments were carried out at five different temperatures, that is, 20, 30, 40, 50, and 60°C. When the desired temperature was reached, about 0.01 g of NbO/g-C₃N₄ was added into flask. The pH effect was also studied. Before mixing with the adsorbent, various pH levels (3.0–11.5) of the dye solution were adjusted by adding a few drops of diluted hydrochloric acid (0.1 M HCl) or sodium hydroxide (0.1 M NaOH).

At the end of the equilibrium period, aqueous sample (3 mL) was taken from the solution and then filtered by syringe filter. The concentration of MB in solution was determined by UV-Vis spectrophotometer at a wavelength of 664 nm. The amount of MB adsorbed at equilibrium q_e (mg g⁻¹) was calculated by following equation:

$$q_e = (C_0 - C_e)V/m \quad (1)$$

Where C_0 (mg L⁻¹) is the initial MB concentration, C_e (mg L⁻¹) is the MB concentration at equilibrium, V (L) is the volume of MB solution, and m (g) is the mass of the adsorbent.

For the kinetic experiments, 0.01 g of NbO/g-C₃N₄ was added into 200 mL of MB solution at different initial concentrations and temperatures. The adsorption capacity q_t (mg g⁻¹) at different adsorb times was calculated by the following equation:

$$q_t = (C_0 - C_t)V/m \quad (2)$$

where C_t (mg L⁻¹) represented the concentration of MB at any time t .

RESULTS AND DISCUSSION

Characterizations of the Adsorbent

XRD powder patterns were carried out to analyze the structures of the prepared g-C₃N₄, NbO, and NbO/g-C₃N₄ materials (see **Figure 1**). Two characteristic peaks at 13.1° and 27.4° were indexed to (100) and (002) planes of pristine g-C₃N₄ (Zhang et al., 2016), and these two peaks can be ascribed to the in-plane structural packing motif of tris-triazine units and the interlayer stacking of aromatic systems, respectively (Zhang et al., 2009). The bottom XRD pattern of NbO could be assigned to the phase of pure NbO (JCPDS 14-0288). The spectrum of NbO/g-C₃N₄ composite shows the diffraction peaks of both g-C₃N₄ and NbO. This indicates that NbO has successfully reacted with g-C₃N₄ sheets and both of them are good in the hybrid composite.

The morphology and structures of the samples were characterized by using both FESEM and TEM (**Figure 2**). **Figure 2A** shows typical FESEM image of sheet structure of pristine g-C₃N₄. It can be seen that the morphology of g-C₃N₄ was irregular and the sizes were different with each other. The FESEM image (**Figure 2B**) of NbO/g-C₃N₄ composite was like a heap of flower-like spheres, which were assembled from plenty curved nanosheets with varied sizes. Moreover, the FESEM image (**Figure 2C**) shows clearly surface structure of the composite. Closer observation demonstrated that the microspheres have highly uniform structure and highly porous texture. The structure of NbO/g-C₃N₄ was completely different

with g-C₃N₄ since the hydrothermal treatment with NbO at 180°C could significantly modified the structure of g-C₃N₄. The changes of the structure can be further confirmed by the TEM images. **Figure 2D** shows the pristine bulk g-C₃N₄ with obvious layer structure. In contrast, TEM image of NbO/g-C₃N₄ (**Figure 2E**) reveal the nanosheets are crumpled, and **Figure 2F** exhibits that the average thickness were ~0.8 nm in the nanosheets, which further indicated its ultrathin thickness.

The FTIR spectra of prepared g-C₃N₄, NbO, and NbO/g-C₃N₄ composite are shown in **Figure 3**. The Nb-O band in the composite is clearly visible in the region 515–900 cm⁻¹, although there is a broad band in the range from 515 to 663 cm⁻¹ compared to the peaks at 507 and 643 cm⁻¹ of NbO. In the spectrum of g-C₃N₄, the broad band around 3150 cm⁻¹ is indicating N-H stretching vibrations, the peaks at 1626 and 1235 cm⁻¹ were corresponding to the C=N and C-N stretching vibrations, respectively. The peak at 805 cm⁻¹ was related to the s-triazine ring vibrations (Kumar et al., 2014). Therefore, all characteristic peaks of NbO and g-C₃N₄ were observed in NbO/g-C₃N₄ composite sample. The UV-vis absorption spectra of g-C₃N₄, NbO, NbO/g-C₃N₄ and the hybrid material after adsorbing MB (NbO/g-C₃N₄-MB) are shown in **Figure S1**.

To gain insight into the real composition and chemical states of g-C₃N₄, NbO, and NbO/g-C₃N₄ hybrid composite, XPS measurements were carried out and the results are exhibited in **Figure 4**. The full survey spectra of g-C₃N₄, NbO, and NbO/g-C₃N₄ were displayed in **Figure 4A**. The presence of Nb, C, N, O, and K elements in NbO/g-C₃N₄ indicated that the hybrid composite have all characteristic elements of g-C₃N₄ and NbO. It's observed that the main peak centered at 284.7 eV from the C 1s spectrum (**Figure 4B**) should be ascribed to the sp² C-C or/and C=C bonds, which originates from the adventitious reference carbon on the surface (Zhang et al., 2012). For the g-C₃N₄ sample, the C 1s peak centered at 288.2 eV was assigned to the sp² carbon atoms bonded to N (N=C-(N)₂) in the graphitic structure. As for the C 1s peaks of NbO/g-C₃N₄ (288.5 and 289.2 eV) emanate from sp² carbon atoms shift to higher banding energy orientation after through hydrothermal treatment, suggesting that the -NH₂ groups of g-C₃N₄ has been replaced by the -OH groups to form an N=C(N)-OH species. Meanwhile, the peaks also can be affected by the Linqvist unit of NbO due to it has strong electronic pull. Therefore, the results indicated that either terminal oxygen atom from Nb=O or bridge oxygen from Nb-O-Nb groups within Linqvist unit have interactions with (N=C-(N)₂) group within g-C₃N₄ or N=C(N)-OH species resulting from hydrothermal treatment. Three main peaks of N 1s spectra can be seen from **Figure 4C**, the main peak centered at 398.7 eV should be corresponding to sp² N atoms involved in tris-triazine rings (C=C-N), and other two main peaks ascribed to tertiary nitrogen (N-(C)₃) (400.0 eV) and N atoms bonded with H atoms (C-N-H) in the aromatic rings (401.0 eV) (Dong et al., 2017). However, the binding energy of the first one in N 1s of the composite (399.3 eV) was found to be slightly bigger than those of g-C₃N₄. The similar situation also can be seen in the C 1s and O 1s. **Figure 4D** shows that g-C₃N₄ sample exhibits O 1s peak at 532.3 eV which can be ascribed to the adsorbed water. Three peaks centered at 532.3, 529.5,

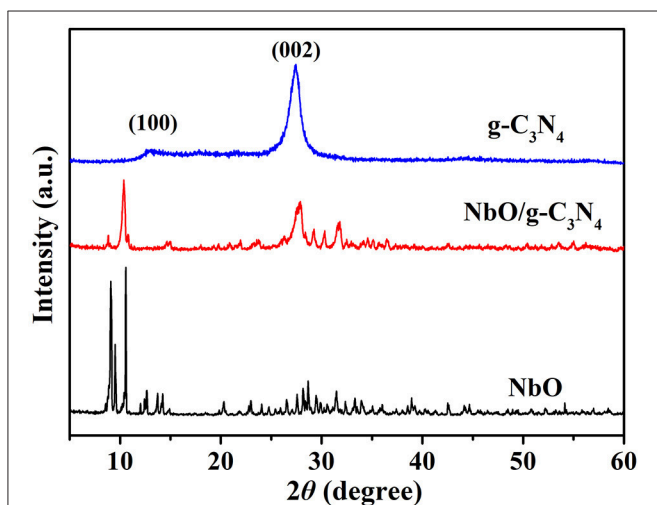


FIGURE 1 | XRD powder patterns of g-C₃N₄, NbO/g-C₃N₄, and NbO.

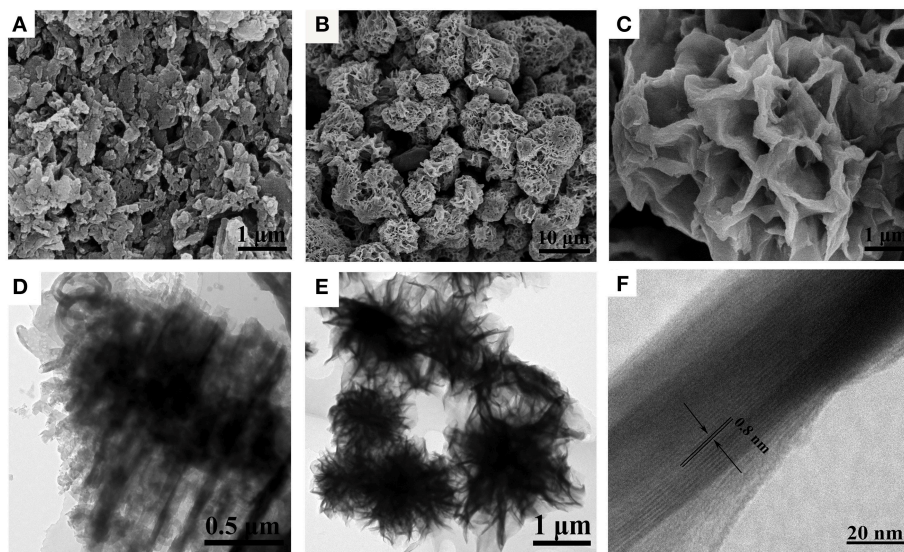


FIGURE 2 | FESEM images of g-C₃N₄ (A), NbO/g-C₃N₄ (B,C), and TEM images of g-C₃N₄ (D), NbO/g-C₃N₄ (E,F).

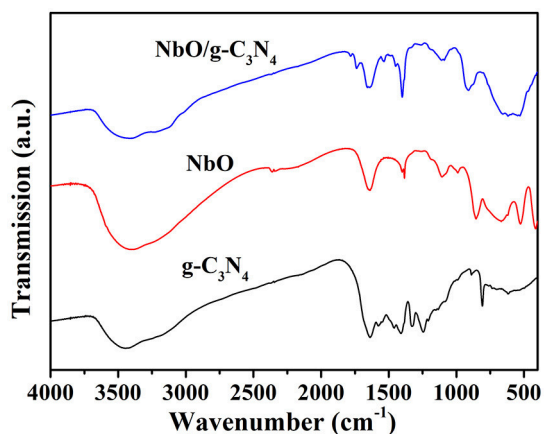


FIGURE 3 | FTIR spectra of g-C₃N₄, NbO, and NbO/g-C₃N₄.

and 531.0 eV were detected on NbO sample, which is assigned to Nb–O–Nb, Nb–O–H, and adsorbed water, respectively. After through the process of hydrothermal treatment, the peak of NbO/g-C₃N₄ in the O 1s has two main peaks. The main peak at 532.2 eV just like g-C₃N₄ and NbO, and the other one is narrow peak which results from the binding energy of different oxygen-containing species. Compared with NbO, the changes of Nb 3d and K 2p binding energy in the NbO/g-C₃N₄ composite (Figures 4E,F) can further confirm the Linqvist unit of NbO sample has interacted with g-C₃N₄ sample.

Effect of Initial Dye Concentration

The time-dependent adsorption experiments toward MB with different initial dye concentration (10, 20, 30, and 40 mg L⁻¹)

were studied on NbO/g-C₃N₄ (see Figure 5). The adsorption capacity of the MB increased with time and then reached equilibrium after 240 min. It can be easily observed that the adsorption is quickly increased in the initial stage. And after 90 min, the increasing trend did not stop but slow down gradually. This phenomenon was not hard to explain, which is due to the fact that the most empty surface on the adsorbents were available during the initial stage and the remaining empty surface sites were hard to occupy due to the repulsive forces between the MB molecules on the NbO/g-C₃N₄ and the bulk phase (Fu et al., 2015). The equilibrium adsorption capacity of MB with increased initial concentrations shows an increasing trend since the increasing MB concentration can provide an increase driving force to overcome the mass transfer resistance of the dye (Konicki et al., 2013). Hence, it indicates that the initial MB concentration has a great influence on the adsorption process.

Effect of Initial pH

The initial pH of solution usually has a significant effect on MB adsorption process. In order to observe the influence, the adsorption experiments were performed in the pH values ranging from 3.0 to 11.5 at MB concentration of 20 mg L⁻¹ and 30°C. The effect of initial pH on the adsorption capacity of MB is given in Figure 6A. The adsorption capacity has a prominent increasing trend from 142.43 to 216.09 mg g⁻¹ when the pH of the dye solution was increased over the whole studied range, which is quite similar to the previous research (El Qada et al., 2006; Xu et al., 2017). The increase of adsorbed MB amount with increasing pH might be due to the fact that the concentration of negative charge of the adsorbent increases with increasing pH (Xu et al., 2017). Hence, pH can be seen as an important factor to the adsorption process. The plot of ΔpH vs. pH_i was given in Figure 6B and the pH at which ΔpH becomes zero

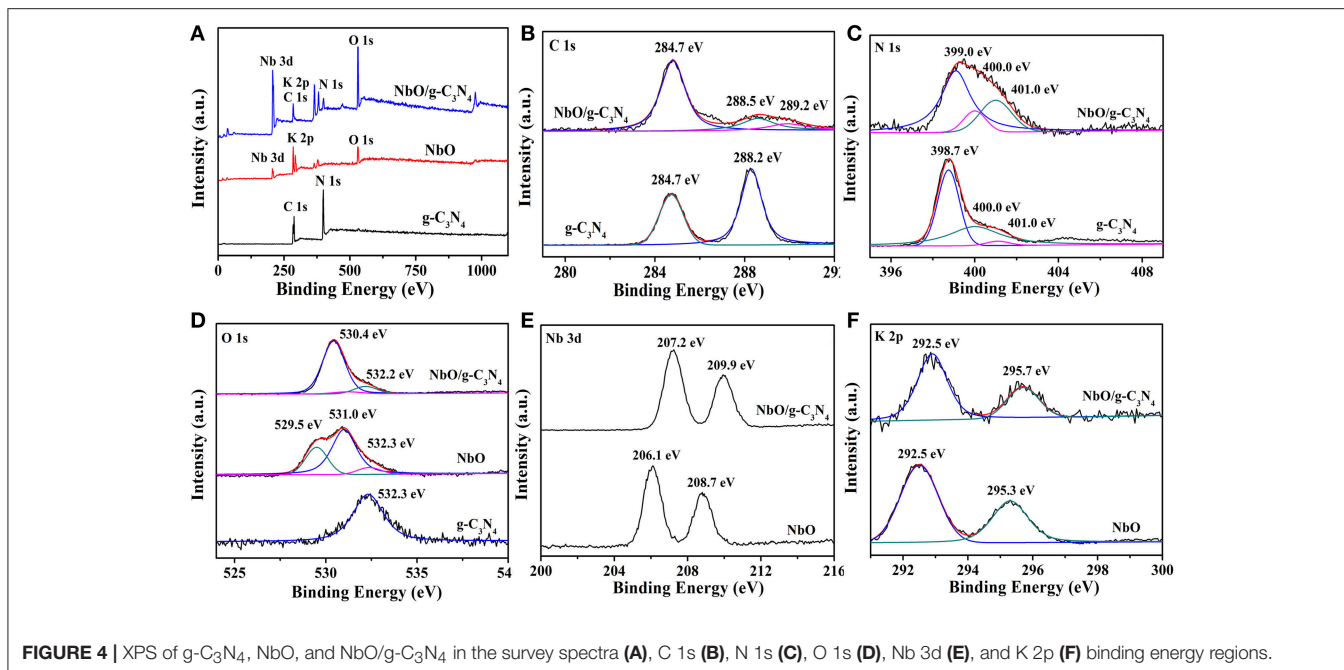


FIGURE 4 | XPS of g-C₃N₄, NbO, and NbO/g-C₃N₄ in the survey spectra (A), C 1s (B), N 1s (C), O 1s (D), Nb 3d (E), and K 2p (F) binding energy regions.

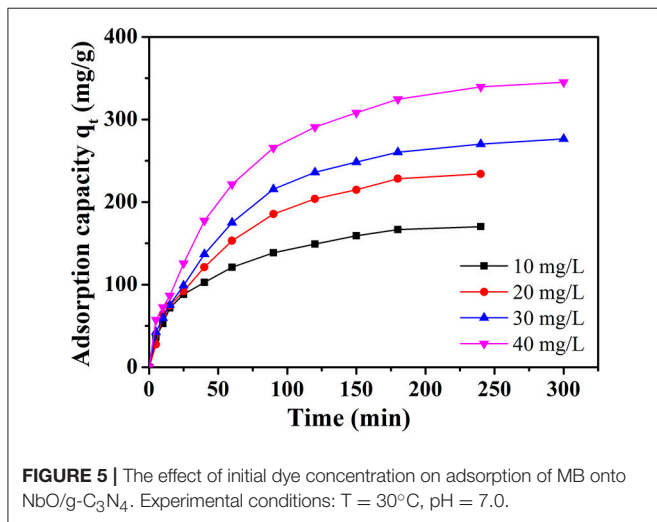


FIGURE 5 | The effect of initial dye concentration on adsorption of MB onto NbO/g-C₃N₄. Experimental conditions: T = 30°C, pH = 7.0.

is called pH_{pzc} . The pH_{pzc} value for NbO/g-C₃N₄ was 6.93 and it is the pH at which the net surface charge on adsorbent is zero. The adsorbent surface has a net positive charge at $pH < pH_{pzc}$, while has a net negative charge at $pH > pH_{pzc}$ (El Qada et al., 2006). It indicates that NbO/g-C₃N₄ surface becomes negatively charged when $pH > 6.93$, and it will be favorite the adsorption of MB in cationic form. Thus, as pH is increased, the adsorbent surface is more negatively charged leading to a biggish attraction between the NbO/g-C₃N₄ and MB. Besides, when the pH is under pH_{pzc} , the NbO/g-C₃N₄ surface is more positively charged, which does not favor the adsorption of dye positive ions because of the electrostatic repulsion.

Effect of Temperature

The amount of adsorption of MB on NbO/g-C₃N₄ with various temperatures is shown in Figure 7. The adsorption capacity of MB was enhanced with increasing temperature, indicated it is an endothermic process. In order to investigate the thermodynamic parameter, variation of Gibbs free energy (ΔG°), enthalpy change (ΔH°), and entropy change (ΔS°) were determined by the following equations:

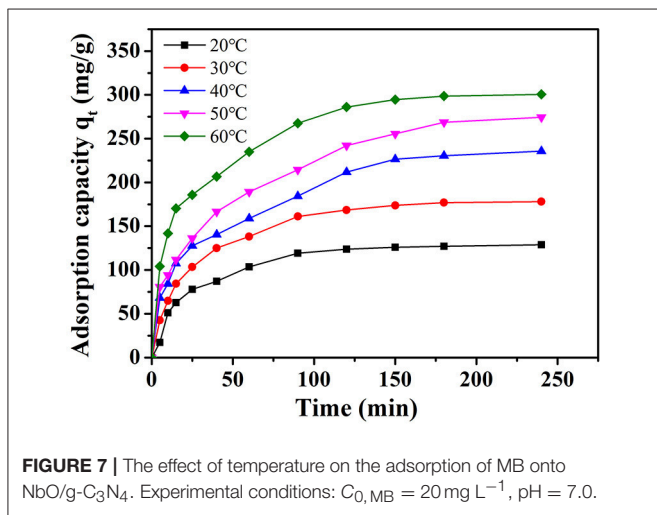
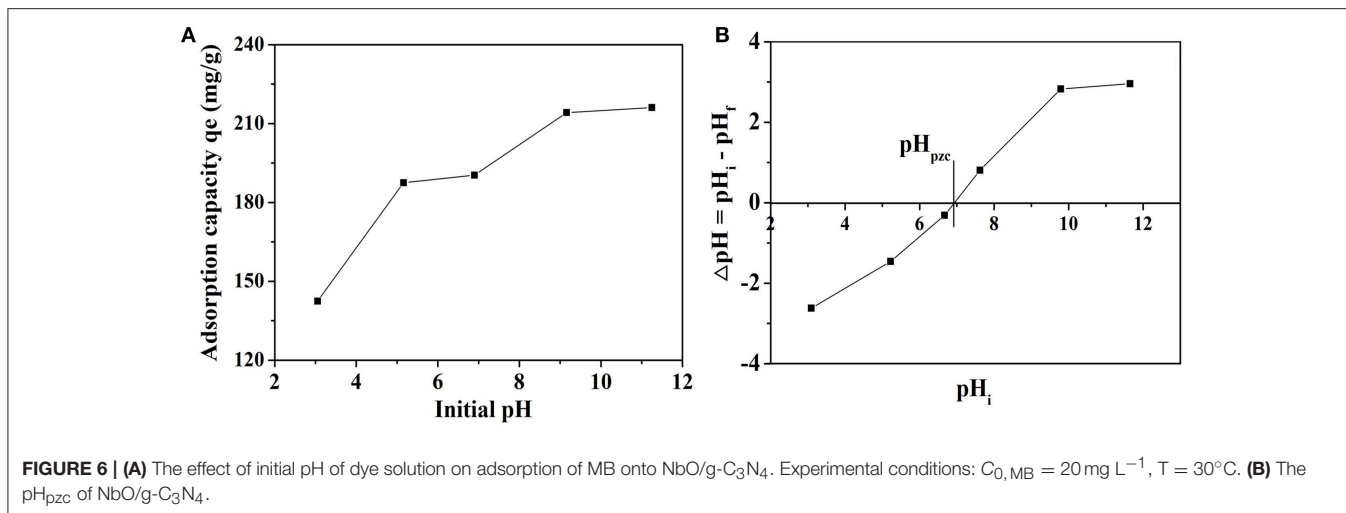
$$\Delta G^\circ = -RT \ln K_a \quad (3)$$

$$K_a = q_e / C_e \quad (4)$$

$$\ln K_a = \Delta S^\circ / R - \Delta H^\circ / RT \quad (5)$$

Where R and T represent the gas constant (8.314 J mol⁻¹ K⁻¹) and the temperature (K), K_a is the adsorption equilibrium constant. The enthalpy (ΔH°) and entropy (ΔS°) can be obtained from the slope and intercept from the Van't Hoff plot of $\ln K_a$ vs. $1/T$ (Figure S2). The values of ΔG° , ΔH° , and ΔS° were calculated and the results are summarized in Table 1.

The negative value of ΔG° (-5.55, -7.14, -8.94, -10.23, and -11.48 kJ mol⁻¹ at 293, 303, 313, 323, and 333 K, respectively) suggest that the adsorption of MB was spontaneous. The positive value of ΔH° (38.3 kJ mol⁻¹) confirms that the adsorption of MB on NbO/g-C₃N₄ is an endothermic process and the value smaller than 40 kJ mol⁻¹ indicates the adsorption is a physical adsorption process (Yao et al., 2010). Furthermore, the positive value of ΔS° (150.2 J mol⁻¹ K⁻¹) indicates that the freedom of the adsorption process was increased in the solid-solution interface. This similar case has also been observed by Fu et al. (2015) and Zheng et al. (2017). Molecules may be restricted on the surface after adsorption and unable to optionally move in three dimensions but as the temperature increased, the motion of molecules obtained free and their disorderliness



increased resulting in the entropy increased. Therefore, all the above thermodynamic parameters represent that NbO/g-C₃N₄ can be used as an effective adsorbent for MB removal in aqueous solution.

Adsorption Isotherms

The adsorption isotherms can be described as: at a fixed temperature, the adsorbates interact with adsorbent when the adsorption processes of solute molecules reach its equilibrium. Hence, adsorption isotherms are necessary parameters to study the adsorption system. Usually, the Langmuir and Freundlich isotherms were used to depict the equilibrium adsorption. The Langmuir isotherm is based on the assumption that adsorption occurs on a homogeneous surface. Meanwhile, the Freundlich isotherm describes the adsorption process which takes place on a heterogeneous surface. The two models are represented by the following equations:

$$C_e/q_e = 1/Q_0b + C_e/Q_0 \quad (6)$$

TABLE 1 | Thermodynamic parameters for adsorption MB onto NbO/g-C₃N₄.

| Dye concentration (mg L ⁻¹) | ΔH° (kJ mol ⁻¹) | ΔS° (J mol ⁻¹ K ⁻¹) | ΔG° at temperature (°C) (kJ mol ⁻¹) | | | | |
|---|--|---|--|-------|-------|--------|--------|
| | | | 20 | 30 | 40 | 50 | 60 |
| 20 | 38.36 | 150.24 | -5.55 | -7.14 | -8.94 | -10.23 | -11.48 |

$$\ln q_e = \ln K_F + 1/n \ln C_e \quad (7)$$

Where C_e represents the equilibrium concentration of MB (mg L^{-1}); q_e and Q_0 represent the adsorption capacity (mg g^{-1}) and the maximum adsorption capacity of MB at equilibrium, respectively. The b is a Langmuir constant (L mg^{-1}) which is related to the adsorption rate. K_F and n are Freundlich constants which are related to the adsorption capacity and intensity, respectively. The essential factor of Langmuir isotherm can be expressed in terms of a dimensionless equilibrium parameter (R_L), which is calculated by the following equation (Hameed et al., 2007):

$$R_L = 1/(1 + bC_0) \quad (8)$$

where C_0 (mg L^{-1}) represents the highest initial dye concentration and b (L mg^{-1}) is Langmuir constant. The value of R_L indicates that the type of the isotherm is either favorable ($0 < R_L < 1$), unfavorable ($R_L > 1$), linear ($R_L = 1$), or irreversible ($R_L = 0$). The calculated value of R_L (0.0056) confirmed that the adsorption of MB on NbO/g-C₃N₄ is favorable.

The value of Q_0 , b , K_F , and n were determined from the slope and intercept of the linear plot C_e/q_e vs. C_e and $\ln q_e$ vs. $\ln C_e$ (Figures 8A,B), and the results are given in the Table 2. The correlation coefficients R^2 (0.9917) of Langmuir model is more close to 1 than that of Freundlich model (0.9501), suggesting the adsorption data fitted well with Langmuir model. In addition, the value of n (4.751 L mg^{-1}) in the range from 1.0 to 10.0 represented a good adsorption process (Chairat et al., 2008).

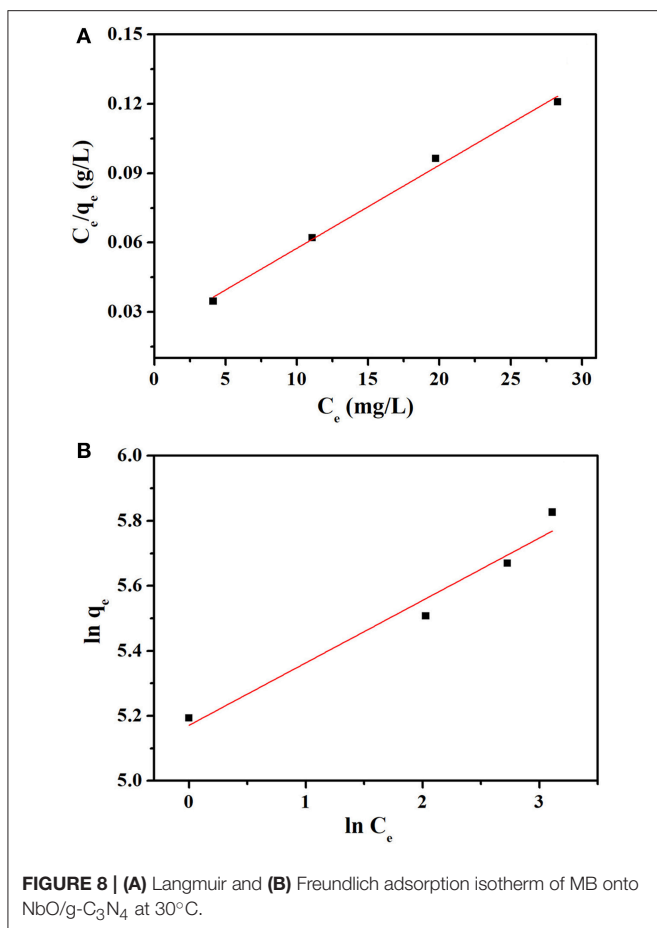


TABLE 2 | Langmuir and Freundlich parameters for MB on NbO/g-C₃N₄.

| LANGMUIR ISOTHERM | |
|--|--------|
| Q_0 (mg g ⁻¹) | 373.13 |
| b (L mg ⁻¹) | 0.4751 |
| R_L | 0.0056 |
| R^2 | 0.9917 |
| FREUNDLICH ISOTHERM | |
| K_F [(mg g ⁻¹)(L mg ⁻¹) ^{1/n}] | 176.07 |
| n | 5.2037 |
| R^2 | 0.9501 |

Maximum adsorption capacities of various adsorbents applied for adsorbed MB reported in the literatures are displayed in **Table 3**. Adsorption capacity of NbO/g-C₃N₄ in this work is higher than that obtained in most of other studies. This data can be confirmed that NbO/g-C₃N₄ is a highly efficient adsorbent in the removal of MB from aqueous solution.

Adsorption Kinetics

In order to completely explore the mechanism of the adsorption of MB on NbO/g-C₃N₄, three different kinetic models (pseudo first order, pseudo second order, and intraparticle diffusion model) were used to analyze the kinetic adsorption data. Pseudo

TABLE 3 | Comparison of the maximum adsorption capacity of MB onto various adsorbents.

| Adsorbent | Q_0 (mg g ⁻¹) | References |
|-------------------------------------|-----------------------------|------------------------|
| Mesoporous carbon nitride | 360.8 | Zhang et al., 2014 |
| MOFs-235 | 187 | Haque et al., 2011 |
| Graphene | 204 | Liu et al., 2012 |
| Hydrolyzed carbon nitride | 402 | Wang et al., 2013 |
| Commercial activated carbon | 200 | Doke and Yadav, 2014 |
| Fe ₃ O ₄ /NPC | 292.4 | Jiao et al., 2016 |
| Halloysite nanotubes | 84.23 | Zhao and Liu, 2008 |
| Mesoporous hybrid xerogel | 144 | Wu et al., 2005 |
| Molybdenum disulfide | 297 | Massey et al., 2016 |
| Hazelnut husk-activated carbon | 476.2 | Karacetin et al., 2014 |
| NbO/g-C ₃ N ₄ | 373.1 | This work |

first order model is represented by the following equation:

$$\ln(q_e - q_t) = \ln q_e - k_1 t \quad (9)$$

where q_e (mg g⁻¹) and q_t (mg g⁻¹) represent the adsorption capacity of MB at equilibrium and at time t . The k_1 (min⁻¹) is the first order rate constant, and the values of k_1 and q_e were calculated from the slope and intercept of the linear plot $\ln(q_e - q_t)$ vs. t , respectively. Meanwhile, the linear plot $\ln(q_e - q_t)$ vs. t at the condition of 30°C and initial pH value (7.0) is given in **Figure S3**. Moreover, pseudo second order model is given by the following equation:

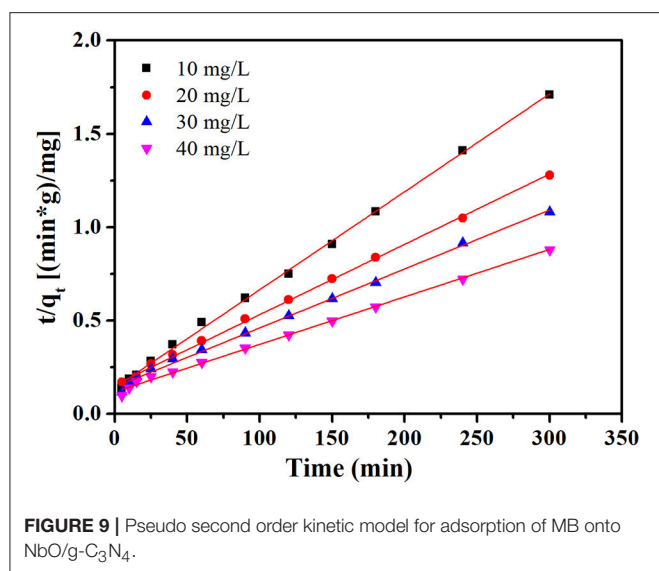
$$t/q_t = 1/k_2 q_e^2 + t/q_e \quad (10)$$

where k_2 (mg g⁻¹ min⁻¹) is the pseudo second order rate constant. The values of k_2 and q_e were obtained from the slope and intercept of the plot of t/q_t vs. t . The plot of t/q_t vs. t at the condition of 30°C and initial pH value (7.0) is given in **Figure 9**. Furthermore, the intraparticle diffusion model suggested by Weber and Borris was thoroughly studied and the equation can be expressed as follows:

$$q_t = k_i t^{0.5} + C \quad (11)$$

where the k_i (mg g⁻¹ min^{-0.5}) is the rate constants for intraparticle diffusion model and C (mg g⁻¹) is the intercept. The value of k_i was determined from the slope of the plot of q_t vs. $t^{0.5}$ (**Figure S4**).

The relevant parameters (k_1 , k_2 , and q_e) of MB adsorption on NbO/g-C₃N₄ from pseudo first order and pseudo second order models are displayed in **Table S1**. It can be seen from the plots of the pseudo second order show a good agreement between the experimental and calculated q_e values for different initial MB concentrations. Moreover, compared to the correlation coefficients of both models, it's obvious that coefficients of pseudo second order model is greater and more near to unity. Hence, it can be concluded that MB adsorption on NbO/g-C₃N₄ is described by pseudo second order model.



The experiment data was also analyzed by the intraparticle diffusion model. The graphs of q_t vs. $t^{0.5}$ can be divided into two regions. First region was explained to diffusion of MB molecules from solution to the external surface of NbO/g-C₃N₄ and second region was diffusion into pores of NbO/g-C₃N₄. As shown in Figure S3, the k_{i1} values were bigger than k_{i2} values indicating the second region of intraparticle diffusion is a gradually process, which fit in with the parameters of intraparticle diffusion displayed in Table S2. Furthermore, because of the plot did not pass through origin, it was indicated that intraparticle diffusion was not rate-controlling step (Duran et al., 2011). So, the adsorption involved by both intraparticle diffusion as well as diffusion to external surface step (Singh and Pant, 2004; Cheung et al., 2007).

CONCLUSIONS

In summary, a NbO/g-C₃N₄ hybrid composite with porous structure was successfully obtained using one-step hydrothermal

REFERENCES

- Bestani, B., Bendorouche, N., Benstaali, B., Belhakem, M., and Addou, A. (2008). Methylene blue and iodine adsorption onto an activated desert plant. *Bioresour. Technol.* 99, 8441–8444. doi: 10.1016/j.biortech.2008.02.053
- Cai, Z. Q., Sun, Y. M., Liu, W., Pan, F., Sun, P. Z., and Fu, J. (2017). An overview of nanomaterials applied for removing dyes from wastewater. *Environ. Sci. Pollut. Res.* 24, 15882–15904. doi: 10.1007/s11356-017-9003-8
- Chairat, M., Rattanaphani, S., Bremner, J. B., and Rattanaphani, V. (2008). Adsorption kinetic study of lac dyeing on cotton. *Dyes Pigments* 76, 435–439. doi: 10.1016/j.dyepig.2006.09.008
- Cheung, W. H., Szeto, Y. S., and McKay, G. (2007). Intraparticle diffusion processes during acid dye adsorption onto chitosan. *Bioresour. Technol.* 98, 2897–2904. doi: 10.1016/j.biortech.2006.09.045

method. The effects of a variety of operating conditions (initial dye concentration, pH, and temperature) were studied. Results indicated that the adsorption of MB is favored at high pH (216.9 mg g⁻¹ at pH = 11.25), and the adsorption capacity of MB increases with increasing initial concentration and temperature. The adsorption data were described by the Langmuir and Freundlich models, and the result suggested the adsorption of MB onto NbO/g-C₃N₄ was fitted well with the Langmuir model and maximum adsorption capacity of NbO/g-C₃N₄ was found to be 373.13 mg g⁻¹. In the adsorption kinetic studies, it was demonstrated that the experiment data was well described by pseudo second order model. Moreover, the intraparticle diffusion model represented that two steps happened during the adsorption process and intraparticle diffusion was not rate-limiting step. The thermodynamic analyses indicated that adsorption MB onto NbO/g-C₃N₄ was a spontaneous endothermic process. Hence, it can be expected that NbO/g-C₃N₄ can be a new class of adsorbent for removing methylene blue from polluted water effectively.

AUTHOR CONTRIBUTIONS

QG: carried out all experiments, did data collection, data analysis, and prepared the manuscript; WS: helped analyze the XPS data; YX: helped explain some of the experimental results and revise manuscript; YH: contributed to the scientific interpretation of results and revised the manuscript.

ACKNOWLEDGMENTS

This work is supported by Shanghai Pujiang Program (15PJ1400200), the Fundamental Research Funds for the Central Universities and the starting up foundation from Donghua University.

SUPPLEMENTARY MATERIAL

The Supplementary Material for this article can be found online at: <https://www.frontiersin.org/articles/10.3389/fchem.2018.00007/full#supplementary-material>

- Doke, S. M., and Yadav, G. D. (2014). Novelty of combustion synthesized titania ultrafiltration membrane in efficient removal of methylene blue dye from aqueous effluent. *Chemosphere* 117, 760–765. doi: 10.1016/j.chemosphere.2014.10.029
- Dong, C. C., Ma, Z. Y., Qie, R. T., Guo, X. H., Li, C. H., Wang, R. J., et al. (2017). Morphology and defects regulation of carbon nitride by hydrochloric acid to boost visible light absorption and photocatalytic activity. *Appl. Catal. B Environ.* 217, 629–636. doi: 10.1016/j.apcatb.2017.06.028
- Duran, C., Ozdes, D., Gundogdu, A., Imamoglu, M., and Senturk, H. B. (2011). Tea-industry waste activated carbon, as a novel adsorbent, for separation, preconcentration and speciation of chromium. *Anal. Chim. Acta* 688, 75–83. doi: 10.1016/j.aca.2010.12.029
- El Qada, E. N., Allen, S. J., and Walker, G. M. (2006). Adsorption of Methylene Blue onto activated carbon produced from steam activated bituminous coal: a study of equilibrium adsorption isotherm. *Chem. Eng. J.* 124, 103–110. doi: 10.1016/j.ccej.2006.08.015

- Fu, J. W., Chen, Z. H., Wang, M. H., Liu, S. J., Zhang, J. H., Zhang, J. N., et al. (2015). Adsorption of methylene blue by a high-efficiency adsorbent (polydopamine microspheres): kinetics, isotherm, thermodynamics and mechanism analysis. *Chem. Eng. J.* 259, 53–61. doi: 10.1016/j.cej.2014.07.101
- Hameed, B. H., Din, A. T. M., and Ahmad, A. L. (2007). Adsorption of methylene blue onto bamboo-based activated carbon: kinetics and equilibrium studies. *J. Hazard. Mater.* 141, 819–825. doi: 10.1016/j.jhazmat.2006.07.049
- Haque, E., Jun, J. W., and Jhung, S. H. (2011). Adsorptive removal of methyl orange and methylene blue from aqueous solution with a metal-organic framework material, iron terephthalate (MOF-235). *J. Hazard. Mater.* 185, 507–511. doi: 10.1016/j.jhazmat.2010.09.035
- He, J. J., Sun, H. Q., Indrawirawan, S., Duan, X. G., Tade, M. O., and Wang, S. B. (2015). Novel polyoxometalate@g-C₃N₄ hybrid photocatalysts for degradation of dyes and phenolics. *J. Colloid Interface Sci.* 456, 15–21. doi: 10.1016/j.jcis.2015.06.003
- Hu, J. C., Song, Z., Chen, L. F., Yang, H. J., Li, J. L., and Richards, R. (2010). Adsorption properties of MgO(111) nanoplates for the dye pollutants from wastewater. *J. Chem. Eng. Data* 55, 3742–3748. doi: 10.1021/je100274e
- Jiao, C. N., Wang, Y. N., Li, M. H., Wu, Q. H., Wang, C., and Wang, Z. (2016). Synthesis of magnetic nanoporous carbon from metal-organic framework for the fast removal of organic dye from aqueous solution. *J. Magn. Magn. Mater.* 407, 24–30. doi: 10.1016/j.jmmm.2016.01.031
- Karacetin, G., Sivrikaya, S., and Imamoglu, M. (2014). Adsorption of methylene blue from aqueous solutions by activated carbon prepared from hazelnut husk using zinc chloride. *J. Anal. Appl. Pyrolysis* 110, 270–276. doi: 10.1016/j.jaap.2014.09.006
- Konicki, W., Sibera, D., Mijowska, E., Lendzion-Bielun, Z., and Narkiewicz, U. (2013). Equilibrium and kinetic studies on acid dye Acid Red 88 adsorption by magnetic ZnFe₂O₄ spinel ferrite nanoparticles. *J. Colloid Interface Sci.* 398, 152–160. doi: 10.1016/j.jcis.2013.02.021
- Kumar, S., Kumar, B., Surendar, T., and Shanker, V. (2014). g-C₃N₄/NaTaO₃ organic-inorganic hybrid nanocomposite: high-performance and recyclable visible light driven photocatalyst. *Mater. Res. Bull.* 49, 310–318. doi: 10.1016/j.materresbull.2013.09.013
- Li, K. X., Yan, L. S., Zeng, Z. X., Luo, S. L., Luo, X. B., Liu, X. M., et al. (2014). Fabrication of H₃PW₁₂O₄₀-doped carbon nitride nanotubes by one-step hydrothermal treatment strategy and their efficient visible-light photocatalytic activity toward representative aqueous persistent organic pollutants degradation. *Appl. Catal. B Environ.* 156, 141–152. doi: 10.1016/j.apcatb.2014.03.010
- Liu, J. H., Xie, S. Y., Geng, Z. B., Huang, K. K., Fan, L., Zhou, W. L., et al. (2016). Carbon nitride supramolecular hybrid material enabled high-efficiency photocatalytic water treatments. *Nano Lett.* 16, 6568–6575. doi: 10.1021/acs.nanolett.6b03229
- Liu, T. H., Li, Y. H., Du, Q. J., Sun, J. K., Jiao, Y. Q., Yang, G. M., et al. (2012). Adsorption of methylene blue from aqueous solution by graphene. *Colloids Surf. B Biointerfaces* 90, 197–203. doi: 10.1016/j.colsurfb.2011.10.019
- Liu, X. X., Gong, W. P., Luo, J., Zou, C. T., Yang, Y., and Yang, S. J. (2016). Selective adsorption of cationic dyes from aqueous solution by polyoxometalate-based metal-organic framework composite. *Appl. Surf. Sci.* 362, 517–524. doi: 10.1016/j.apsusc.2015.11.151
- Liu, Y. P., Guo, S. X., Ding, L., Ohlin, C. A., Bond, A. M., and Zhang, J. (2015). Lindqvist polyoxoniobate ion-assisted electrodeposition of cobalt and nickel water oxidation catalysts. *ACS Appl. Mater. Interfaces* 7, 16632–16644. doi: 10.1021/acsami.5b04219
- Long, Z. Y., Zhou, Y., Chen, G. J., Ge, W. L., and Wang, J. (2014). C₃N₄-H₅PMo₁₀V₂O₄₀: a dual-catalysis system for reductant-free aerobic oxidation of benzene to phenol. *Sci. Rep.* 4, 5. doi: 10.1038/srep03651
- Massey, A. T., Gusain, R., Kumari, S., and Khatri, O. P. (2016). Hierarchical microspheres of MoS₂ nanosheets: efficient and regenerative adsorbent for removal of water-soluble dyes. *Ind. Eng. Chem. Res.* 55, 7124–7131. doi: 10.1021/acs.iecr.6b01115
- Moussavi, G., and Mahmoudi, M. (2009). Removal of azo and anthraquinone reactive dyes from industrial wastewaters using MgO nanoparticles. *J. Hazard. Mater.* 168, 806–812. doi: 10.1016/j.jhazmat.2009.02.097
- Osugi, M. E., Rajeshwar, K., Ferraz, E. R. A., De Oliveira, D. P., Araujo, A. R., and Zanoni, M. V. B. (2009). Comparison of oxidation efficiency of disperse dyes by chemical and photoelectrocatalytic chlorination and removal of mutagenic activity. *Electrochim. Acta* 54, 2086–2093. doi: 10.1016/j.electacta.2008.07.015
- Peng, J., Zhang, W., Liu, Y., Jiang, Y., Ni, L., and Qiu, J. (2017). Superior adsorption performance of mesoporous carbon nitride for methylene blue and the effect of investigation of different modifications on adsorption capacity. *Water Air Soil Poll.* 228:9. doi: 10.1007/s11270-016-3189-0
- Singh, T. S., and Pant, K. K. (2004). Equilibrium, kinetics and thermodynamic studies for adsorption of As(III) on activated alumina. *Sep. Purif. Technol.* 36, 139–147. doi: 10.1016/S1383-5866(03)00209-0
- Troupis, A., Hiskia, A., and Papaconstantinou, E. (2002). Synthesis of metal nanoparticles by using polyoxometalates as photocatalysts and stabilizers. *Angew. Chem. Int. Ed.* 41, 1911–1912. doi: 10.1002/1521-3773(20020603)41:11<1911::AID-ANIE1911>3.0.CO;2-0
- Wang, H., Gao, H. H., Chen, M. X., Xu, X. Y., Wang, X. F., Pan, C., et al. (2016). Microwave-assisted synthesis of reduced graphene oxide/titania nanocomposites as an adsorbent for methylene blue adsorption. *Appl. Surf. Sci.* 360, 840–848. doi: 10.1016/j.apsusc.2015.11.075
- Wang, X. C., Blechert, S., and Antonietti, M. (2012). Polymeric graphitic carbon nitride for heterogeneous photocatalysis. *ACS Catal.* 2, 1596–1606. doi: 10.1021/cs300240x
- Wang, Y. B., Hong, J. D., Zhang, W., and Xu, R. (2013). Carbon nitride nanosheets for photocatalytic hydrogen evolution: remarkably enhanced activity by dye sensitization. *Catal. Sci. Technol.* 3, 1703–1711. doi: 10.1039/c3cy20836b
- Wu, H. L., Zhang, Z. M., Li, Y. G., Wang, X. L., and Wang, E. B. (2015). Recent progress in polyoxoniobates decorated and stabilized via transition metal cations or clusters. *Crystengcomm* 17, 6261–6268. doi: 10.1039/C5CE00909J
- Wu, Z. J., Joo, H., and Lee, K. (2005). Kinetics and thermodynamics of the organic dye adsorption on the mesoporous hybrid xerogel. *Chem. Eng. J.* 112, 227–236. doi: 10.1016/j.cej.2005.07.011
- Xiao, L., Xiong, Y., Tian, S. H., He, C., Su, Q. X., and Wen, Z. H. (2015). One-dimensional coordination supramolecular polymer Cu(bipy)(SO₄)_n as an adsorbent for adsorption and kinetic separation of anionic dyes. *Chem. Eng. J.* 265, 157–163. doi: 10.1016/j.cej.2014.11.134
- Xin, L., Jin, A. L., Jia, Y. S., Xia, T. L., Deng, C. X., Zhu, M. H., et al. (2017). Synergy of adsorption and visible-light photocatalytic degradation of methylene blue by a bifunctional Z-scheme heterojunction of WO₃/g-C₃N₄. *Appl. Surf. Sci.* 405, 359–371. doi: 10.1016/j.apsusc.2017.02.025
- Xu, S., Lv, Y., Zeng, X., and Cao, D. (2017). ZIF-derived nitrogen-doped porous carbons as highly efficient adsorbents for removal of organic compounds from wastewater. *Chem. Eng. J.* 323, 502–511. doi: 10.1016/j.cej.2017.04.093
- Yan, Z. X., Zhu, B. C., Yu, J. G., and Xu, Z. H. (2016). Effect of calcination on adsorption performance of Mg-Al layered double hydroxide prepared by a water-in-oil microemulsion method. *RSC Adv.* 6, 50128–50137. doi: 10.1039/C6RA05253C
- Yao, Y. J., Xu, F. F., Chen, M., Xu, Z. X., and Zhu, Z. W. (2010). Adsorption behavior of methylene blue on carbon nanotubes. *Bioresour. Technol.* 101, 3040–3046. doi: 10.1016/j.biortech.2009.12.042
- Zhang, J. S., Zhang, M. W., Zhang, G. G., and Wang, X. C. (2012). Synthesis of carbon nitride semiconductors in sulfur flux for water photoredox catalysis. *ACS Catal.* 2, 940–948. doi: 10.1021/cs300167b
- Zhang, S. W., Zeng, M. Y., Li, J. X., Li, J., Xu, J. Z., and Wang, X. K. (2014). Porous magnetic carbon sheets from biomass as an adsorbent for the fast removal of organic pollutants from aqueous solution. *J. Mater. Chem. A* 2, 4391–4397. doi: 10.1039/C3TA14604A
- Zhang, Y. J., Thomas, A., Antonietti, M., and Wang, X. C. (2009). Activation of carbon nitride solids by protonation: morphology changes, enhanced ionic conductivity, and photoconduction experiments. *J. Am. Chem. Soc.* 131, 50–51. doi: 10.1021/ja808329f
- Zhang, Y. Y., Zhou, Z. X., Shen, Y. F., Zhou, Q., Wang, J. H., Liu, A. R., et al. (2016). Reversible assembly of graphitic carbon nitride 3D network for highly selective dyes adsorption and regeneration. *ACS Nano* 10, 9036–9043. doi: 10.1021/acsnano.6b05488

- Zhao, M. F., and Liu, P. (2008). Adsorption behavior of methylene blue on halloysite nanotubes. *Microporous Mesoporous Mater.* 112, 419–424. doi: 10.1016/j.micromeso.2007.10.018
- Zhao, S., Zhao, X., Zhang, H., Li, J., and Zhu, Y. F. (2017). Covalent combination of polyoxometalate and graphitic carbon nitride for light-driven hydrogen peroxide production. *Nano Energy* 35, 405–414. doi: 10.1016/j.nanoen.2017.04.017
- Zheng, Y. Q., Zhu, B. C., Chen, H., You, W., Jiang, C. J., and Yu, J. G. (2017). Hierarchical flower-like nickel(II) oxide microspheres with high adsorption capacity of Congo red in water. *J. Colloid Interface Sci.* 504, 688–696. doi: 10.1016/j.jcis.2017.06.014

Conflict of Interest Statement: The authors declare that the research was conducted in the absence of any commercial or financial relationships that could be construed as a potential conflict of interest.

Copyright © 2018 Gan, Shi, Xing and Hou. This is an open-access article distributed under the terms of the Creative Commons Attribution License (CC BY). The use, distribution or reproduction in other forums is permitted, provided the original author(s) and the copyright owner are credited and that the original publication in this journal is cited, in accordance with accepted academic practice. No use, distribution or reproduction is permitted which does not comply with these terms.